ELSEVIER

Journal of Hazardous Materials A137 (2006) 88–98

Journal of Hazardous Materials

www.elsevier.com/locate/jhazmat

Investigation of entrainment and thermal properties of a cryogenic dense-gas cloud using optical measurement techniques

J.P. Kunsch *, T. Rösgen

Institute of Fluid Dynamics, ETH Zurich, 8092 Zurich, Switzerland

Received 21 December 2005; received in revised form 24 February 2006; accepted 27 February 2006
Available online 18 April 2006

Abstract

Cryogenic dense-gas clouds have been investigated in a heavy-gas channel under controlled source and ambient conditions. Advantage is taken from new, non-intrusive optical measurement techniques (e.g. image correlation velocimetry, ICV, and background oriented Schlieren, BOS) providing detailed pictures of the temperature and velocity field in relevant regions of the cloud. The ice particles in the cloud, formed by nucleation, represent a natural seeding to be used as tracers, which have the advantage of behaving passively. Two layers can be identified in a cryogenic gas cloud: a lower cold layer, which is visible due to the presence of ice particles, and an invisible upper layer, where the ice particles have melted, mostly due to heat addition by air entrainment into the upper layer.

A two-layer model has been applied to a generic element of the cloud, where detailed experimental data regarding velocity and temperature are available. Thermal- and dilution behaviour can be interpreted by means of the model which is presented in detail. A global entrainment parameter is deduced allowing a simple comparison with existing experimental information obtained by other traditional experimental techniques. The numerical values of the present entrainment parameter agree well with the correlations proposed by other authors. Thermal effects, such as heat transfer from the ground, appear to be very important. In addition, the visible height of the cloud can be predicted in relative good agreement with the experimental observations, by means of a thermal balance including the phase transition of the ice particles.

Keywords: Dense-gas dispersion; Cryogenic; Dilution; Entrainment; Optical measurement techniques

1. Introduction

Cold gas clouds from cryogenic sources are relevant, e.g. in the context of the transportation and storage of cryogenic gases (LNG, LPG, etc.) for energy purposes. Several experiments were motivated by the early interest in the related hazards. The Maplin Sands trials with LNG and refrigerated liquefied propane (Puttock et al. [1]) or the Burro Series LNG experiments (Ermak et al. [2]) should be mentioned in the context of large-scale field trials. Only the first experiment of the Burro trials was performed with LN_2, which evaporated on a water surface, the other eight trials were performed with LNG. These experiments provided a better insight into the basic physical phenomena including the thermal behaviour and have been used repeatedly for code validation. Nielsen and Ott [3] show the significance and time dependence of heat transfer in large-scale heavy-gas dispersion using field data, e.g. of the Desert Tortoise or Burro trials. Recent large-scale field experiments performed with liquid hydrogen evaporating and spreading on complex terrain with buildings show that this issue is still very topical and that detailed experimental information is still necessary for the validation of theoretical models and software packages (Statharas et al. [4]). The experimental data confirm the strong effect of ground heating on the propagation and dilution dynamics. The additional parameters, which are involved when heat transfer effects are present, however, represent a major difficulty in establishing workbook correlations yielding, e.g. concentrations versus distance from the source (Britter and McQuaid [5]).

In contrast to field trials the wind tunnel experiments facilitated a detailed investigation of the heat transfer effects from the ground, which are crucial for the spreading and dilution behaviour of cryogenic or cold gases (Kunsch and Fanneløp [6], Kumar et al. [7]). In case of a continuous release, quasi-steady state asymptotic experimental data for the relevant properties of

* Corresponding author. Tel.: +41 44 632 26 42; fax: +41 44 632 11 47.
E-mail address: kunsch@ifd.mavt.ethz.ch (J.P. Kunsch).

0304-3894/$ – see front matter © 2006 Elsevier B.V. All rights reserved.
doi:10.1016/j.jhazmat.2006.02.053

Nomenclature

a	$a = \lambda/\rho c_p$
b	width of the channel
c_f	friction coefficient
c_p	specific heat at constant pressure
g	acceleration of gravity
H	height of the cloud
H_s	visible height of the cloud
i	enthalpy
$\dot{m}$	mass flow rate
p	pressure (p_s saturation vapour pressure)
Pr	Prandtl number
$\dot{Q}$	heat flux
$\dot{q}$	heat flux per unit area
r_i	latent heat of fusion
r_s	latent heat of evaporation
Re	Reynolds number
Ri	Richardson number
T	temperature
u	velocity
v_e	entrainment velocity
x	location in the channel
x_i	mass fraction of ice ($x_i = \dot{m}_i/\dot{m}_a$)
x_a	humidity ratio, specific humidity

Greek letters

α	heat transfer coefficient
β	entrainment coefficient
β_e	volume coefficient of expansion
γ	isentropic exponent, ratio of specific heats
φ	relative humidity
λ	thermal conductivity
μ	dynamic viscosity
ν	kinematic viscosity
ρ	density
τ	shear stress

Subscripts/superscripts

a	air
ae	entrained air, ambient
B	characterizes the ground surface (e.g. temperature of the ground surface T_B)
f	film (cf. T_f: film temperature)
i	ice
iv	ice/water vapour (cf. $\dot{m}_{iv}$: mass flow rate undergoing phase transition)
s	source
v	water vapour

the cloud can be obtained after the initially high heating rates of the cloud due to heat-transfer from the ground. One of the first wind tunnel facilities, which was suited for the continuous release of various cold gases is described in Andreiev et al. [8] or Neff et al. [9]. The authors include data of their own laboratory trials and of other authors on turbulent entrainment, which depends on stratification expressed by a Richardson number.

The present contribution deals with a continuous release of cryogenic nitrogen in the heavy-gas channel of the IFD at ETHZ. The simple geometry and a well defined source element or spill section ensure a one-dimensional quasi-steady (planar) flow. New non-intrusive optical methods, such as image correlation velocimetry (ICV, e.g. Tokumaru and Dimotakis [10]) and background oriented Schlieren (BOS, e.g. Meier [11], Dalziel et al. [12]), can be applied, making use of light sheet optics and a CCD camera capturing the pictures through the transparent side walls. Similar experiments, dealing with one-dimensional planar channel flows from a continuous LN_2 source, but making use of traditional measuring techniques, are reported by Ruff et al. [13] and Poag [14]. Both contributions contain experimental data, e.g. on the heat transfer rates from the ground surface or the dilution behaviour by entrainment. This information is used for comparison with the present experimental results and for validation of the present theoretical model. The model considered here includes a momentum- and energy balance and is formulated for a generic differential element or "control volume" in the heavy-gas channel, where detailed experimental data at the inlet and at the outlet is available. This information, including the velocity data, can be used in the momentum balance to obtain an entrainment parameter with a value in the range found by Ruff et al. [13] and which is in agreement with the correlation proposed by Poag [14]. A good identification of the visible height of the cloud, corresponding to the lower layer containing the ice particles, is possible by means of the imaging techniques. In the present model, the upper mixing layer and the lower colder layer (delimited by the visible height) are treated separately. A distinction is made between the heat flux contributing to the phase transition, i.e. the melting of the ice particles, and the surface heat flux contributing mainly to the heating of the lower layer.

2. Experimental investigation

2.1. Experimental setup

Among other experiments, the heavy-gas channel at IFD was used to study the continuous release of cryogenic liquid nitrogen and the spreading of the evaporated dense-gas cloud. The heat required for the evaporation is provided by immersion heaters in a Dewar containing the LN_2. This mode of evaporation can be described as "dry evaporation" because only the humidity of the entrained ambient air contributes to the ice formation, in contrast to experiments using evaporation over a water surface.

The channel (Fig. 1) has a total length of 12 m, is 1.2 m wide and has an open top to prevent mutual intrusion effects. The transparent side walls facilitate the application of the optical measurement techniques. The Dewar is located at the centre of the release chamber having a length of 1.28 m. It can be observed that the flow is already roughly planar when leaving the release chamber. The axis of the channel has its origin in the centre of the Dewar and the positions where the measurements are performed, as given in the present text, are located on this axis. The experiments reported here are performed in the second horizon-

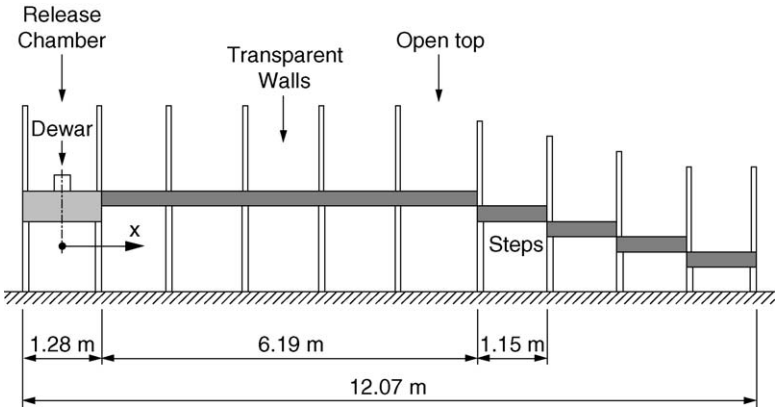

Fig. 1. Schematic view of the heavy-gas channel at ETH.

tal section. The third section consists of a series of consecutive steps which can be compared to idealized topographic features and which provide a downstream control of the flow. Special attention is paid to the distance between the control volume in the horizontal section considered here for modeling purposes and the first step, which must be sufficient to prevent a perception of the downstream features at the measurement positions.

The ice particles formed in the cloud are small enough to act as discrete, passive tracers and can be used as natural seeding for flow visualization. The sinking speed under the influence of gravity is estimated to be smaller than 1 mm/s. Furthermore, the comparatively low particle density renders the cloud practically transparent to optical (and thermal) radiation. This simplifies the overall energy balance and allows a direct identification of the remaining contributing effects.

In order to facilitate the distributed, simultaneous measurements of flow properties required for a global energy balance, it was decided to use non-intrusive optical imaging techniques wherever possible. This led to the measurement of temperature fields using a computerized variant of the classical Schlieren technique, the extraction of flow velocities based on image correlation velocimetry and the determination of the cloud's visible height using an image integration and segmentation algorithm.

2.2. Optical temperature measurements

The temperature of the cloud is measured using a background oriented Schlieren method (BOS). It is based on the spatially resolved measurement of image distortions, which are created by optical density variations in the line-of-sight of a camera focused on an optimized target pattern. In the case of the semi-transparent cryogenic gas cloud, strong temperature gradients lead to such refractive index variations as described by the Gladstone–Dale relationship

$$n - 1 = k\rho = k\frac{p_0}{RT} \tag{2.1}$$

For the second equality, a height-averaged constant pressure p_0 can be taken with a good approximation in the ideal gas relationship. The BOS technique registers local image distortions which are related to the gradients of the refractive index, as integrated along the line-of-sight in the test section (Fig. 2). Thus, the technique provides depth-averaged data and is best suited for the analysis of essentially two-dimensional flows.

In the present case, the temperature field in the vertical plane is derived from the equation

$$T = k\frac{p_0}{R}\frac{1}{n-1} = \frac{k'}{n-1} \tag{2.2}$$

Taking into account the integration constant required for the integration of the measured gradient field, one arrives at the solution for the temperature field

$$T = \frac{1}{k_1 n + k_2} \tag{2.3}$$

This equation indicates that two constants have to be inserted to obtain an absolute temperature field. In the experiments, the wall and ambient temperatures at two discrete points are inserted, giving finally

$$k_1 = \frac{T_a^{-1} - T_w^{-1}}{n_a - n_w}; \quad k_2 = T_w^{-1} - k_1 n_w \tag{2.4}$$

Fig. 2 shows typical results of the temperature profiles over height, which are obtained by thermocouple measurements at different distances from the source element and which are used

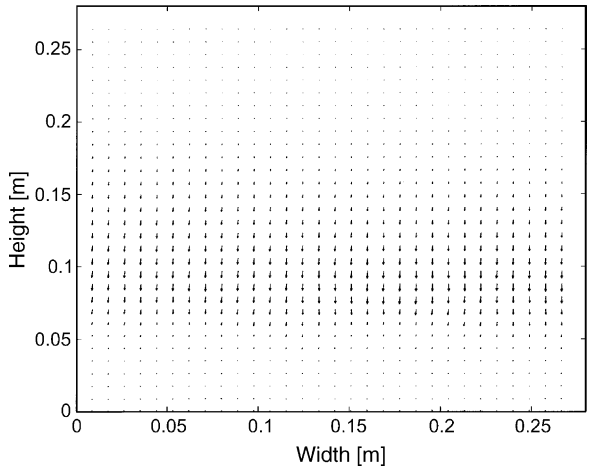

Fig. 2. Vector field representing the gradient of the refractive index; integration of the gradient field yields the temperature field.

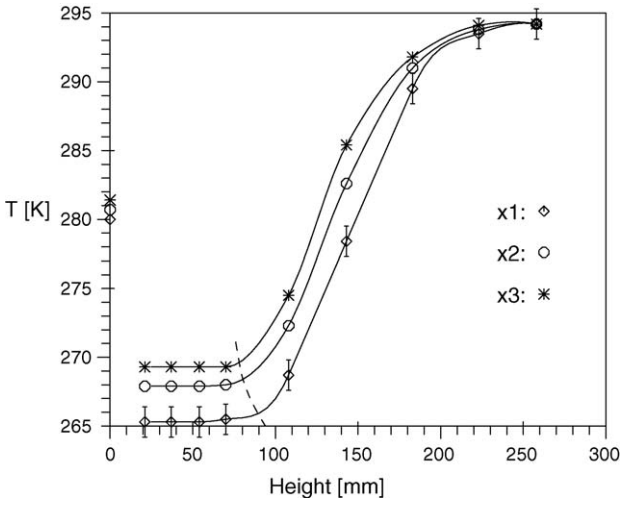

Fig. 3. Temperature distribution over the height of the cloud obtained by thermocouple measurements, the bars indicate the relative difference to the measurements by the BOS imaging technique (for three locations x_1, x_2 and x_3; x_1 and x_3 are the inlet and the outlet of the control volume, respectively).

as a reference. (Location x_1 and x_3 correspond to the inlet and the outlet, respectively, of the generic differential control volume defined for modeling purposes.) The vertical error bars indicate the maximum relative difference of the distributions obtained by the BOS imaging technique and the thermocouple measurements, respectively (illustrated, e.g. by means of the distribution at the inlet x_1 of the control volume). With a relative difference not exceeding 2%, the agreement of both distributions can be considered as very good.

The temperature in the lower layer of the dense-gas cloud is constant to a good approximation, indicating intense mixing during the free convection process. The temperature at the ground surface (zero height in Fig. 3) has been recorded by thermocouples, which are mounted along the centreline of the channel flush with the ground surface. With this information the heat transfer from the floor into the cloud can be estimated. It can be observed in the experiments that the height of the visible lower layer of the cryogenic cloud roughly corresponds to the kink in the temperature distribution in Fig. 3, where the temperature increases.

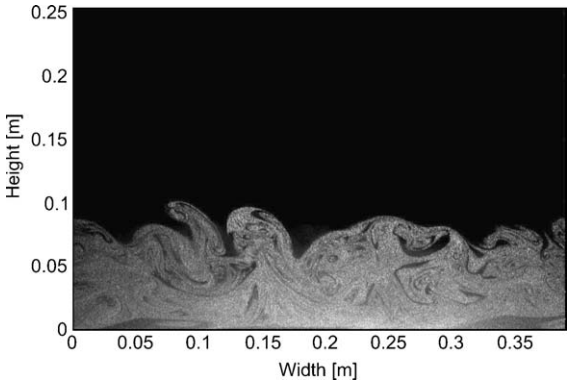

Fig. 4. Snapshot of the flow field illuminated with a light sheet.

2.3. Optical velocity measurements

Making use of the ice particles in the cloud as tracers, an image velocimetry technique was employed to measure the flow velocities in a vertical cross-section of the flow. For this, a pulsed laser illuminated a thin section (sheet) of the flow (Fig. 4). A digital camera synchronized with the laser then recorded two image frames in rapid succession. Any local motion between the images was then detected by a pattern matching/correlation algorithm and translated back to velocities.

The "dry" evaporation process constrains the seeding density in a range which is not well suited for regular particle image velocimetry (PIV), where the optical resolution of individual (ice) particles is required. For a given image magnification – defined by the need to view the whole cloud height – the tracers cannot be resolved and thus their motion cannot be analyzed directly. Nevertheless, naturally occurring variations in the seeding density are readily visible as distinctive brightness features and can be used to determine the local convection velocity. This velocimetry technique, known as image correlation velocimetry (ICV), is used to derive velocities inside the cryogenic cloud. Outside the "visible" cloud, where the ice particles have evaporated due to the higher temperatures, a separate seeding using talcum powder was used to extend the velocimetry measurements. A detailed description of the velocimetry technique can be found in Jensen et al. [15].

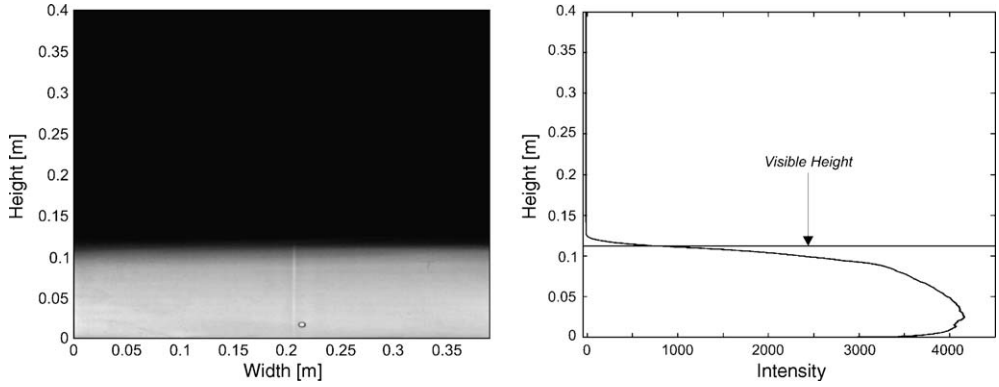

Fig. 5. Light intensity profile for detecting the visible height of the cloud (average of 150 images).

The results indicate that the velocity field has essentially a "top-hat" shape, showing a nearly constant value throughout the cloud including especially the visible region. In order to simplify the theoretical analysis of the cloud behaviour, such constant values were used for the inlet and the outlet plane of the control volume of the present model.

2.4. Measurement of the visible cloud height

The fact that the ice particles evaporate rapidly once the local temperature exceeds a certain threshold value close to the freezing point can be used for another simple yet effective measurement. The "visible" cloud height and its change along the flow are linked to the local heat exchange and phase transition inside the cloud and thus provide an additional verification of the theoretical model's validity.

From an image analysis point of view, the identification of the visible height reduces to the task of defining and detecting a suitable threshold in the recorded image brightness. In order to eliminate the influence of the visible density fluctuations on the height estimate, a large number of images (150) are averaged. Looking at the vertical intensity profiles in these images, a sharp change in brightness can be observed and the vertical coordinate of the strongest gradient is defined as the location of the visible edge (Fig. 5).

3. Model development

3.1. Dilution behaviour: estimate of the entrainment parameter

Two locations at two different distances from the LN_2 source or Dewar are chosen, where the temperature profiles over the height and the velocity distributions are measured. The measuring techniques, i.e. ICV for the velocity profiles and BOS or thermocouples for the temperature profiles, have been described in Sections 2.2 and 2.3. The temperature of the surface of the floor is measured by means of thermocouples which are incorporated into the surface where the cloud spreads. This information is required to estimate the heat flux from the floor into the cloud. The temperature and the moisture of the ambient air are measured by means of a commercial thermometer and hygrometer, respectively. With this information, a control volume can be defined (Fig. 6) where the velocity and temperature profiles are measured in the inlet- and the outlet planes and the temperature distributions on the top and on the bottom of the cloud. This control volume can be considered as a generic "differential element", because the quantities, such as temperature or velocity, vary continuously and relatively slowly with the distance from the source. For reasons of simplicity, no distinction is made between the properties of nitrogen and air (79% of nitrogen).

The equation of continuity is formulated for the generic control volume represented in Fig. 6 for the different components

$$\text{air}: \quad \frac{\mathrm{d}\dot{m}_\mathrm{a}}{\mathrm{d}x}\,\mathrm{d}x = \dot{m}_\mathrm{ae} \tag{3.1}$$

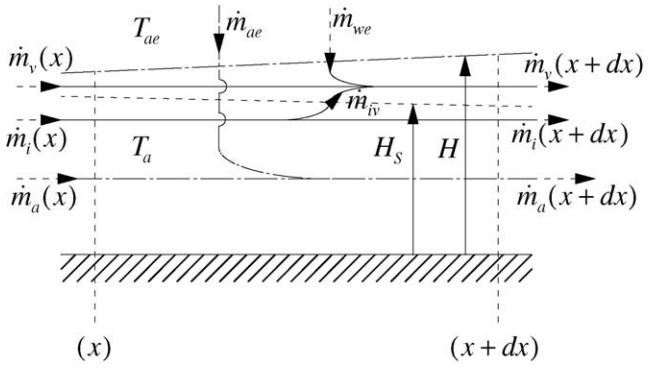

Fig. 6. Generic differential "control volume".

$$\text{ice}: \quad \frac{\mathrm{d}\dot{m}_\mathrm{i}}{\mathrm{d}x}\mathrm{d}x = -\dot{m}_\mathrm{iv} \tag{3.2}$$

$$\text{water vapour}: \quad \frac{\mathrm{d}\dot{m}_\mathrm{v}}{\mathrm{d}x}\mathrm{d}x = \dot{m}_\mathrm{iv} + \dot{m}_\mathrm{we} \tag{3.3}$$

where $\dot{m}_\mathrm{a}$, $\dot{m}_\mathrm{v}$ and $\dot{m}_\mathrm{i}$ are the mass flow rates of air, water vapour and ice, respectively. $\dot{m}_\mathrm{iv}$ is related to the phase transition of ice particles. $\dot{m}_\mathrm{ae}$ is the mass flow of air entrained into the element with length dx.

$$\dot{m}_\mathrm{ae} = \rho_\mathrm{ae} v_\mathrm{e} b\,\mathrm{d}x \tag{3.4}$$

Since the shear between the cloud and the ambient air is responsible for mixing, the entrainment velocity v_e can be modeled as a function of the difference of the streamwise velocities in the cloud and the (calm) environment. In the simplest variant, the entrainment velocity is proportional to a height-averaged horizontal velocity in the cloud and the constant of proportionality is an entrainment factor β

$$v_\mathrm{e} = \beta u \tag{3.5}$$

Due to the ambient humidity, a mass flow rate of water $\dot{m}_\mathrm{we}$ is entrained into the cloud

$$\dot{m}_\mathrm{we} = x_\mathrm{a}\dot{m}_\mathrm{ae} \tag{3.6}$$

The humidity ratio x_a is related to the relative humidity φ (see, e.g. Moran and Shapiro [16]), i.e.

$$x_\mathrm{a} = 0.622\frac{\varphi p_\mathrm{s}(T)}{p - \varphi p_\mathrm{s}(T)} \tag{3.7}$$

with the saturation vapour pressure p_s.

The momentum balance in horizontal direction for the control volume yields (Jirka [17])

$$\frac{\mathrm{d}}{\mathrm{d}x}\left[\rho H u^2 - \frac{1}{2}g(\rho_\mathrm{ae} - \rho)H^2\right] = -\tau = -c_\mathrm{f}\frac{1}{2}\rho u^2 \tag{3.8}$$

where τ denotes the friction on the ground surface. The corresponding friction factor c_f will be discussed in the section devoted to the empirical input.

By means of the mass- and momentum balance an explicit expression for the entrainment parameter β can be obtained, as

outlined in Appendix A

$$\beta = \frac{1}{c_1}\frac{T_{ae}}{T_a}\left[c_4 H \frac{1}{u}\frac{du}{dx} + c_3 H \frac{1}{T_a}\frac{dT_a}{dx} - \frac{1}{2}c_f u^2\right] \tag{3.9}$$

with $c_1 = u^2 + gH(1 - T_a/T_{ae})$, $c_3 = gH(T_a/T_{ae} - 0.5)$ and $c_4 = -u^2 + gH(1 - T_a/T_{ae})$.

The energy balance for the control volume is

$$\frac{d}{dx}(\dot{m}_a i_a + \dot{m}_v i_v + \dot{m}_i i_i)\,dx = \dot{m}_{ae} i_{ae} + \dot{m}_{we} i_{we} + \dot{Q} \tag{3.10}$$

By evaluating the different terms it can be shown that the terms related to heating or cooling of the water vapour or ice can be neglected, as compared to the dominating terms describing the phase transition.

After some simplifications, which are outlined in detail in Appendix A, the energy balance yields an expression for the temperature gradient in the horizontal direction

$$\frac{H}{T_a}\frac{dT_a}{dx} = \beta\left(1 - \frac{T_a}{T_{ae}}\right) - \frac{\dot{m}_{iv}}{\dot{m}_a}\frac{H}{dx}\frac{r_s + r_i}{c_p T_a} + \frac{\gamma - 1}{\gamma}\frac{\dot{q}}{pu} \tag{3.11}$$

where $\dot{q}$ is the heat flux from the floor per unit area. The interpretation is straightforward: the air and the nitrogen in the cloud are heated up due to the entrainment of ambient air (first term RHS) and the heat transfer from the ground surface (third term RHS). On the other hand, the energy needed for the fusion process of the ice and the subsequent evaporation is extracted from the air and nitrogen in the cloud and contributes to their cooling (second term RHS).

The mass fraction of ice $x_i = \dot{m}_i/\dot{m}_a$ varies due to the melting of the ice and air entrainment during the spreading process, i.e.

$$\frac{dx_i}{dx} = -\beta\left[\left(1 - \frac{T_a}{T_{ae}}\right)\frac{c_5}{H} + \frac{x_i}{H}\frac{T_a}{T_{ae}}\right] + \frac{c_5}{T_a}\frac{dT_a}{dx} - \frac{\gamma - 1}{\gamma}\frac{\dot{q}}{pu}\frac{c_5}{H} \tag{3.12}$$

The mass fraction of ice at the inlet of the control volume can be estimated by means of

$$x_i = x_{is} + \frac{dx_i}{dx}l \tag{3.13}$$

where x_{is} is the mass fraction of ice after completion of the source process and dx_i/dx corresponds to the melting of ice particles by the heat of entrained air during the spreading process over the distance l which corresponds to the distance from the source to the inlet of the generic element.

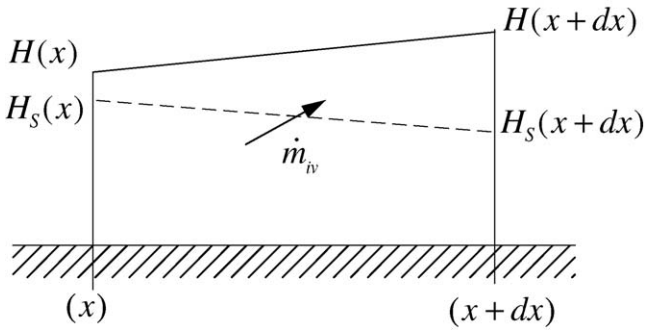

Fig. 7. Evolution of the visible height H_s of the cloud.

3.2. Evolution of the visible height H_s of the cloud

The visible height of the cloud decreases due to the melting of the ice particles.

Eq. (3.2), which is related to the phase transition of the ice particles, can be substituted into Eq. (3.11) to give

$$\frac{1}{\dot{m}_i}\frac{d\dot{m}_i}{dx} = -\frac{c_5}{x_i}\frac{1}{H}\beta\left(1 - \frac{T_a}{T_{ae}}\right) + \left[\frac{c_5}{x_i}\left(\frac{1}{T_a}\frac{dT_a}{dx} - \frac{\gamma - 1}{\gamma}\frac{\dot{q}}{Hpu}\right)\right] \tag{3.14}$$

An indication for the mass flow rate of the ice particles $\dot{m}_i$ is the visible height H_s of the cloud, as suggested in Fig. 7. Hence, H_S can be estimated reasonably well by means of the following equation

$$\frac{1}{H_s}\frac{dH_s}{dx} = \frac{1}{\dot{m}_i}\frac{d\dot{m}_i}{dx} \tag{3.15}$$

By evaluating Eq. (3.14) with the experimental information available, it can be shown that the first term on the RHS dominates over the term within the square parentheses. This suggests that the temperature increase of the cloud can mostly be attributed to the heat transferred from the ground into the cloud. The heat needed for the observed phase transition or melting of the ice particles on the other hand mainly stems from the heat added by entrainment. Making use of these observations, an approximate expression for the evolution of the visible height can be deduced from Eq. (3.15)

$$\frac{dH_s}{dx} = -\frac{c_5}{x_i}\frac{H_s}{H}\beta\left(1 - \frac{T_a}{T_{ae}}\right) \tag{3.16}$$

3.3. Empirical model input and assumptions

3.3.1. Mass fraction of ice particles at the inlet of the control volume

The total mass flux of nitrogen, air, water vapour and ice $\dot{m}$ is composed of the mass flux released at the cryogenic source $\dot{m}_s$ and the mass flux entrained during the source process $\dot{m}_{as}$, and during the spreading process $\dot{m}_{ae}$, i.e.

$$\dot{m} = \dot{m}_s + \dot{m}_{as} + \dot{m}_{ae} \tag{3.17}$$

The existence of ice and water vapour in the cloud can be attributed exclusively to entrainment, because the source process takes place in a Dewar with a dry surface. The heat needed for the evaporation of the LN_2 is provided by immersed heaters. An intense boiling process and a relatively opaque cloud emerging from the Dewar can be observed. This can be explained by the complete freezing of the ambient humidity entrained during the source process, with the temperature of the cloud emerging from the Dewar being less than −80 °C. The quantity of ice after the

source process is accordingly

$$\dot{m}_{is} = x_a \dot{m}_{as} \tag{3.18}$$

The mass fraction of ice x_{is} after completion of the source process can be written by means of Eqs. (3.17) and (3.18)

$$x_{is} \cong \frac{\dot{m}_{is}}{\dot{m}_s + \dot{m}_{as}} = x_a \left(1 - \frac{\dot{m}_s}{\dot{m} - \dot{m}_{ae}}\right) \tag{3.19}$$

$\dot{m}_{ae}$ can be estimated by means of Eqs. (3.4) and (3.5), whereas $\dot{m}_s$ and $\dot{m}$ are determined experimentally.

3.3.2. Friction on the floor

Friction effects for turbulent flow over aerodynamically smooth surfaces can be described by means of the local friction factor $c'_f = 0.0592(Re_x)^{-1/5}$ with Reynolds number $Re_x = ux/\nu$ (see, e.g. Schlichting [18]). An average friction factor c_f can be derived by averaging c'_f between the locations x_1 and x_3, defining the inlet and the outlet of the control volume, i.e.

$$c_f = \frac{1}{x_3 - x_1} \int_{x_1}^{x_3} c'_f \, dx \tag{3.20}$$

For the viscosity, a mean value, depending on the height-averaged temperatures at the inlet and the outlet of the control volume, is taken. (Analogous results may be obtained for wall jets with c_f depending on the Re number, Abrahamson [20].) In reality, c_f as given by Eq. (3.20) is valid for turbulent flow without significant stratification, as opposed to the present heavy-gas dispersion. However, the value $c_f = 0.0064$ obtained is in reasonable agreement with the range suggested by Britter [19] for heavy-gas dispersion over aerodynamically smooth surfaces with free convection effects. It is clear that the value obtained has to be considered as a first approximation, but it will be accepted here for lack of better information. On the other hand, it is felt that a better accuracy for c_f is not required, considering the uncertainties of the other empirical inputs.

3.3.3. Heat transfer from the ground

The heat transfer from the surface of the floor is governed by free convection. The basic parameter is the Rayleigh number $Ra = Gr \cdot Pr$ depending on the Grashof number related to stratification. The heat-transfer coefficient is accordingly (Holman [21] or Britter [19])

$$\alpha = 0.15 \left(\frac{g\beta_e \, \Delta T \rho^2 c_p \lambda^2}{\mu}\right)^{1/3} \tag{3.21a}$$

and the heat flux per unit area is

$$\dot{q} = \alpha \, \Delta T \tag{3.21b}$$

The film temperature is given by $T_f = 0.5(T_a + T_B)$ and $\Delta T = T_a - T_B$. T_a is the temperature in the top-hat profile above the film and the floor temperature T_B is measured by means of the thermocouples incorporated in the ground surface. The properties of the gas (mainly air) depend on the temperature of the film T_f. It can be shown that the heat fluxes predicted by means of Eq. (3.21a) and (3.21b) are in qualitative agreement with the values obtained in previous experiments (Zumsteg [22]).

Table 1
Experimental data at the inlet x_1 and the outlet x_3 of the control volume

	Location x_1	Location x_3
x (m)	2.95	5.20
T_a (K)[a]	265.4	269.1
T_B (K)	280.0	281.4
u (m/s)	0.229	0.238
H_s (m)	0.090	0.078

[a] Value in the plateau or top-hat profile, as shown in Fig. 3.

An approximate expression of the Stanton number for the heat transfer by forced convection $St \cong c_f/2$ is given here for comparison. The corresponding heat transfer coefficient $\alpha_{forc.c.} = 0.5 c_f \rho c_p u$ can be compared to the heat transfer coefficient by free convection Eq. (3.21a) by means of their ratio

$$r_\alpha = \frac{\alpha_{free\,c.}}{\alpha_{forc.c.}} = \frac{0.30(ag\beta_e \, \Delta T/Pr)^{1/3}}{c_f u} \tag{3.22}$$

It will be shown that the numerical value of r_α is large indicating that the heat transfer mechanisms by free convection dominate.

3.3.4. Heat transfer by radiation

Gases, such as nitrogen or oxygen do practically not absorb radiation as opposed to water vapour, which can absorb a certain part of the incoming radiation (Holman [21]). The mass fraction of water entrained during "dry evaporation" (i.e. evaporation in a Dewar without heat transfer from a water surface), however, is only related to the humidity of the ambient air and is hence relatively small. In this case, the cloud can be considered as transparent for radiation. As a consequence the incoming radiation crosses the cloud, heats up the floor and contributes indirectly to the heating of the cloud. This contribution is taken into account by the convective heat transfer from the floor.

4. Results

The experimental information available at the inlet and at the outlet of the control volume is listed in Table 1. The mass flow rate of the cryogenic source is $\dot{m}_s = 9.6$ g/s (±2%). A height of the cloud which is consistent with the top-hat assumptions of the model can be defined by the inflection point of the temperature profile in Fig. 3. Fig. 3 yields an average value for the control volume equal to $H \cong 0.135$ m. At the inflection point the temperature corresponds roughly to the average of the temperature T_a in the plateau and the ambient temperature T_{ae}. The ambient temperature is about $T_{ae} = 294$ K (±0.2%) and the average relative humidity during the experiments is equal to $\varphi = 33.5\%$ yielding a water content in the entrained air $x_a = 0.0051$.

The entrainment parameter is easily estimated by means of Eq. (3.9)

$$\beta = 0.0028$$

By neglecting the ground friction c_f the entrainment parameter would amount to $\beta = 0.0038$. The effect of ground friction appears to be reasonably small, motivating its neglect in older

prediction methods (e.g. Fanneløp and Jacobsen [23]). In case of stable stratification, the influence of c_f would be even smaller. The value of the entrainment parameter is moderately sensitive to the height H: a range of H from 0.130–0.150 m corresponds to a range of β from 0.0025–0.0034. This range is relatively narrow because the entrainment parameter has been derived using velocity and temperature gradients, which are accurately measured, instead of the gradient of the height, which cannot be determined with sufficient accuracy.

The mass fraction x_{i1} of the ice particles at the inlet of the control volume and its variation in the cloud dx_i/dx, as estimated by Eqs. (3.13) and (3.12), respectively, are

$$x_{i1} = 0.0033 \quad \text{and} \quad \frac{dx_i}{dx} = -2.4 \times 10^{-4}\,(1/\text{m})$$

dx_i/dx is rather small, so that x_{i1} is still close to the ice content of the cloud, corresponding to the entrainment of moisture into the cloud during the source process.

Eq. (3.15) yields an estimate of the spatial gradient or slope of the visible height

$$\frac{dH_s}{dx} = -0.0030 \pm 0.0010$$

The inaccuracy in the definition and the experimental determination of the height H is responsible for the uncertainty of ±30%. The simplified Eq. (3.16), which is based on the assumption that the heat needed for the temperature increase of the cloud corresponds to the heat transferred from the ground, provides a rough estimate of the slope of the visible height $dH_s/dx = -0.0049$. The good agreement of this estimate with the experimental value suggests the simplifications leading to Eq. (3.16), but more detailed and accurate experimental information is required for a final confirmation.

The theoretical values can be compared to the experimental result obtained by a visualization method of the cloud, where a section of the cloud is illuminated by a light sheet. The pictures are captured with a CCD camera and an intensity profile is generated as a function of the distance from the ground surface. The visible height corresponds to a sharp, well defined gradient in the intensity profile. The accuracy has been enhanced by generating an average image, which consists of an average of 150 frames. This information is summarized, e.g. in the variation of the visible height yielding a value equal to

$$\frac{dH_s}{dx} \cong -0.0050$$

which is in qualitative agreement with the value predicted by the model.

Additionally, Fig. 3 can be used as an illustration for the evolution of the visible height: here the temperature is recorded over the height of the cloud with the help of thermocouples and by means of the BOS imaging technique. The visible zone with ice particles corresponds to a plateau in the temperature profile ending with a kink, which indicates the visible height. After the kink, the temperature increases drastically with height. The plateau is due to intense mixing by free convection. When the visible height, corresponding to the slope $dH_s/dx \cong -0.0050$ found experimentally, is represented by means of a dashed line (- - -) in Fig. 3, the plausibility of this result appears clearly.

5. Discussion

5.1. Present results, comparison with other data

A major result of the present study is the evaluation of the entrainment parameter, which is relevant for the understanding of the mixing and dilution of heavy-gas clouds. The present value of the entrainment parameter $\beta = 0.0028$, is in agreement with the experimental range $\beta = 0.0028$–0.0037 obtained by Ruff et al. [13]. It must be pointed out that these results have been obtained in a completely different facility. The water content of the cryogenic cloud evaporating over a water surface was much higher and hence the cloud contained a large mass fraction of ice which was not transparent for radiation. In addition, Ruff et al. [13] estimated the entrainment coefficient β by means of an energy balance.

In the experimental correlations for the entrainment velocity v_e (cf. Poag [14], Spicer and Havens [24]), the strong influence of the heat transfer into a cloud clearly appears. A bulk Richardson number, which takes the stratification into account, is defined as follows:

$$Ri_* = g\left(\frac{\rho - \rho_{ae}}{\rho_{ae}}\right)\frac{H_{eff}}{v_*^2}.$$

The velocity scale $v_* = (u_*^2 + 0.25w_*^2)^{1/2}$ contains a convective velocity scale w_* defined by $w_* = [(g/T)(\dot{q}/\rho c_p)H]^{1/3}$ in addition to the friction velocity u_* relevant for shear-generated turbulence, which also occurs in isothermal flows. The heat flux $\dot{q}$ from the ground surface is responsible for unstable stratification and mixing. The velocity scales of the present experiments

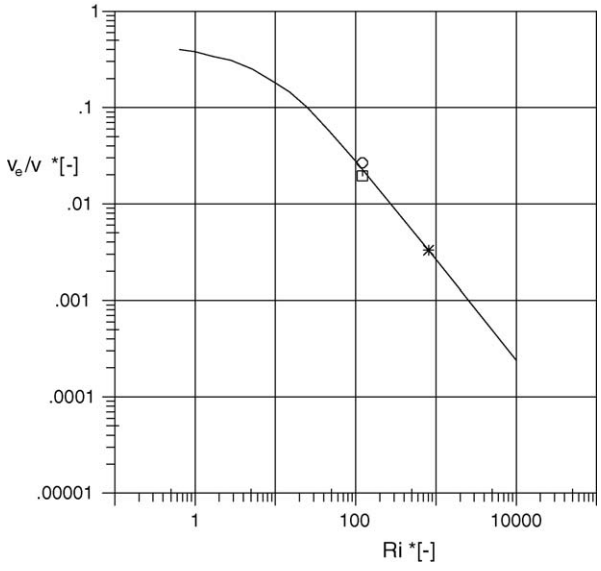

Fig. 8. Scaled entrainment velocity v_e/v_* vs. bulk Richardson number Ri_* correlation of [14], [24]: (—); model result (ground friction neglected): (◯); model result (ground friction taken into account): (□); value given by the correlation for an adiabatic ground surface: (*).

$u_* = 0.013$ m/s and $w_* = 0.061$ m/s yield a Richardson number equal to 121. The correlation of Poag [14] yields a scaled entrainment velocity $v_e/v_* = 0.023$, which corresponds to an entrainment parameter $\beta \cong 0.00324$. Both variants of the present model, neglecting or taking ground friction into account, are compared to the correlation of Poag [14] in Fig. 8. It appears that the values of the present experiment ($\beta = 0.0028$ when the ground friction is taken into account, $\beta = 0.0038$ when c_f is neglected) fall within the range of scatter of the data used for the correlation.

However, when the heat transfer from the floor is neglected, i.e. when $w_* = 0$, the correlation yields $\beta_i \cong 0.00018$. The correct value is one order of magnitude larger (about 20 times) indicating the importance of thermal effects (cf. also Kunsch and Fanneløp [6], Nielsen and Ott [3]). The substantial discrepancy for β, as would be predicted by the correlation for an adiabatic ground surface, is illustrated by the symbol '*' in Fig. 8.

Information on the visible height of the cloud is important for several reasons. Since the ice or visible particles are used as tracers, experimental imaging methods are only suitable for the visible part of the cloud. For this reason the upper layer of the cloud, with temperatures exceeding the freezing point, is not accessible with this kind of measurements. In a first approach, an isotherm close to $T_a = 273$ K could be chosen as an alternative for the experimental definition of the visible top of the cloud. According to Fig. 3, the isotherm would have a slope equal to $dH_T/dx = -0.010$. This value roughly differs by a factor of two from the value observed experimentally for the visible height. However, when heat and mass transfer processes are modeled adequately, as shown in the present contribution, a better estimate of the visible height should be possible. So, the development of the top surface of the visible cloud is closely related to the energy balance of the cloud. In particular, the decay of the mass fraction of ice particles or tracers has been estimated. The mass of the ice particles melting during their journey through the control volume considered in the present experiments amounts to about 15% of the initial mass of ice at the inlet of the volume.

5.2. Scaling considerations: relative importance of free and forced convection

The ratio of the heat transfer coefficients for free and forced convection Eq. (3.22) yields a value $r_\alpha = 5.0$ for the present experiments indicating a clear dominance of free convection effects. Considering the different quantities in Eq. (3.22), it can be shown that this value cannot be maintained in full scale. When modeling is correct, the temperatures and the physical properties should be the same in the model and at full scale. For the following reasoning it will be assumed that the same c_f is valid in the model and at full scale. This can be achieved experimentally with reasonable accuracy. Equality of Froude numbers ensuring that buoyancy effects are correctly modeled, however, yields larger velocities at full scale, so that the relative importance of free and forced convection effects is reduced according to Eq. (3.22). A full-scale scenario, which is ten times larger than the laboratory model, would yield a ratio $r_\alpha = 1.6$ indicating a reduced heat transfer by free convection effects in full scale. When the same similarity requirements are applied to the ratio of the convective velocity scale and the velocity scale for shear-generated turbulence, we obtain

$$\left(\frac{w_*}{u_*}\right)_{\text{f.s.}} = \left(\frac{H_m}{H_{\text{f.s.}}}\right)^{1/6} \left(\frac{w_*}{u_*}\right)_m \tag{3.23}$$

with index f.s. for full scale and index m for the model.

The explanation given in the context of r_α is valid here too. The relative importance of the convective velocity scale decreases with increasing dimensions. This is in line with Britter's conclusions [19] that proper modeling of dense-gas scenarios is not possible when heat transfer effects by free convection dominate.

However, an answer to the question, how sensitive the relative velocity scale v_*/u_* is to the ratio w_*/u_*, would allow a comparison of entrainment data within a limited range of channel dimensions. The relative velocity scale v_*/u_* may be written in full scale with Eq. (3.23)

$$\left(\frac{v_*}{u_*}\right)_{\text{f.s.}} = \left[1 + 0.25\left(\frac{w_*}{u_*}\right)^2_{\text{f.s.}}\right]^{1/2} = \left[1 + 0.25\left(\frac{H_m}{H_{\text{f.s.}}}\right)^{1/3}\left(\frac{w_*}{u_*}\right)^2_m\right]^{1/2} \tag{3.24}$$

For geometric scales ranging from the present model channel dimensions to ten times larger facilities (or release scenarios), v_*/u_* ranges from 2.60 to 1.90, corresponding to a maximum deviation of 25% from the value obtained in the present channel. (The magnification by a factor of ten would cover almost the whole range of plausible experimental facilities with a maximum distance of the source to the outlet of the control volume as large as 50 m.) The range of v_*/u_* appears to be relatively narrow, due to the weak dependence of w_*/u_* on H (as suggested by Eq. (3.23)), so that a value $v_*/u_* = 2.60$ could even be acceptable for considerably larger dimensions. When a friction factor according to Eq. (3.20) is taken, instead of a constant c_f, w_*/u_* would be an even weaker function of the height scale. The present approximation for v_*/u_* appears to be reasonable in light of the correlation of Fig. 8, where the scaled entrainment velocity and the bulk Richardson number exhibit a range of three to four orders of magnitude, in addition to the scatter of the experimental data used for the correlation.

6. Conclusions

Optical methods have been applied to investigate the spreading and dilution behaviour of cryogenic heavy-gas clouds generated in the heavy-gas channel of the IFD at ETHZ. The natural seeding by ice particles, which are generated by nucleation of the surrounding moisture during the evaporation process of the cryogenic cloud, has been used successfully as tracers for image correlation velocimetry ICV. The temperature distributions have been evaluated from the index of refraction measured by a background oriented Schlieren method BOS. A visualization of the

velocity field by means of talcum powder has been achieved for the upper layer of the cloud, where the ice particles melt due to the heat addition by entrainment.

The velocity- and temperature distributions, as obtained by ICV and BOS at the inlet and the outlet of a control volume containing a representative or generic part of the heavy-gas layer, can be used to formulate a mass- and energy balance to estimate the entrained air relevant for the dilution process. The entrainment parameter lies within the range obtained by Ruff et al. [13], who applied different experimental techniques to cryogenic nitrogen flows. In addition, the parameter is in close agreement with the correlation suggested by Poag [14] and Spicer and Havens [24].

The present experiments demonstrate the applicability of optical methods in stratified gas flows, when passive tracers, such as ice particles, are used. They allow a direct measurement of the velocity field and hence a more detailed analysis of relevant structures of a dense-gas cloud, as opposed to the "traditional" techniques, where information on velocity is often deduced from the concentration or temperature fields (obtained, e.g. by aspirated hot wires and thermocouples, respectively).

Appendix A

A.1. Solution procedure

Eqs. (3.1)–(3.3) for mass conservation of air, water vapour and ice are added to obtain

$$\frac{\mathrm{d}\dot{m}}{\mathrm{d}x}\,\mathrm{d}x = (1 + x_\mathrm{a})\dot{m}_\mathrm{ae} \tag{A.1}$$

$\dot{m}$ is the total mass flow rate which varies due to the entrainment of moist air

$$\dot{m} = \dot{m}_\mathrm{a} + \dot{m}_\mathrm{i} + \dot{m}_\mathrm{v} = \rho u H b \tag{A.2}$$

Eq. (A.1) yields with Eqs. (3.4) and (3.7)

$$\frac{\mathrm{d}}{\mathrm{d}x}\left(\frac{\rho}{\rho_\mathrm{ae}} H u\right) \cong \beta u \tag{A.3}$$

The properties of nitrogen and air are similar and the moisture content of the cloud is negligible for continuity considerations. In this case, we obtain

$$\frac{\mathrm{d}}{\mathrm{d}x}\left(\frac{T_\mathrm{ae}}{T_\mathrm{a}} H u\right) \cong \beta u \tag{A.4}$$

The LHS of the equation of continuity (A.4) is differentiated term by term to obtain

$$\beta = \frac{T_\mathrm{ae}}{T_\mathrm{a}} H \left(\frac{1}{u}\frac{\mathrm{d}u}{\mathrm{d}x} + \frac{1}{H}\frac{\mathrm{d}H}{\mathrm{d}x} - \frac{1}{T_\mathrm{a}}\frac{\mathrm{d}T_\mathrm{a}}{\mathrm{d}x}\right) \tag{A.5}$$

The LHS of the momentum balance in the horizontal direction (3.8) is differentiated term by term to obtain

$$\frac{1}{H}\frac{\mathrm{d}H}{\mathrm{d}x} = \frac{c_2}{c_1}\frac{1}{T_\mathrm{a}}\frac{\mathrm{d}T_\mathrm{a}}{\mathrm{d}x} - \frac{2}{c_1} u \frac{\mathrm{d}u}{\mathrm{d}x} - \frac{1}{c_1}\frac{c_\mathrm{f}}{2}\frac{1}{H}u^2 \tag{A.6}$$

with $c_1 = u^2 + gH(1 - T_\mathrm{a}/T_\mathrm{ae})$ and $c_2 = u^2 + 0.5\,gH$.

When Eq. (A.6) is substituted into Eq. (A.5), β is obtained explicitly as a function of the temperature and the velocity gradient in the x direction

$$\beta = \frac{1}{c_1}\frac{T_\mathrm{ae}}{T_\mathrm{a}}\left[c_4 H \frac{1}{u}\frac{\mathrm{d}u}{\mathrm{d}x} + c_3 H \frac{1}{T_\mathrm{a}}\frac{\mathrm{d}T_\mathrm{a}}{\mathrm{d}x} - \frac{1}{2} c_\mathrm{f} u^2\right] \tag{A.7}$$

with $c_3 = gH(T_\mathrm{a}/T_\mathrm{ae} - 0.5)$ and $c_4 = -u^2 + gH(1 - T_\mathrm{a}/T_\mathrm{ae})$.

The LHS of the energy balance Eq. (3.10) is differentiated term by term. It gives using Eqs. (3.1)–(3.3)

$$\left(\dot{m}_\mathrm{a}\frac{\mathrm{d}i_\mathrm{a}}{\mathrm{d}x} + \underline{\dot{m}_\mathrm{v}\frac{\mathrm{d}i_\mathrm{v}}{\mathrm{d}x}} + \underline{\dot{m}_\mathrm{i}\frac{\mathrm{d}i_\mathrm{i}}{\mathrm{d}x}}\right)\mathrm{d}x = \dot{m}_\mathrm{ae}[(i_\mathrm{ae} - i_\mathrm{a}) + \underline{x_\mathrm{a}(i_\mathrm{we} - i_\mathrm{v})}] - \dot{m}_\mathrm{iv}(i_\mathrm{v} - i_\mathrm{i}) + \dot{Q} \tag{A.8}$$

The underlined terms are related to the ice and the water vapour, whose mass is small compared to the total mass of nitrogen or air in the cloud. These terms, which describe the heating or the cooling of ice and water vapour, are neglected in a first approximation. However, the term describing the phase transition of $\dot{m}_\mathrm{iv}$ cannot be neglected. The enthalpies of water vapour i_v and ice i_i are, respectively

$$i_\mathrm{v} = r_\mathrm{s} + c_{pw}(T - 273) \tag{A.9a}$$

$$i_\mathrm{i} = -r_\mathrm{i} + c_{pi}(T_\mathrm{a} - 273) \tag{A.9b}$$

The difference between these enthalpies is in a first approximation

$$i_\mathrm{v} - i_\mathrm{i} \cong r_\mathrm{s} + r_\mathrm{i} \tag{A.10}$$

because the latent heat of evaporation $r_\mathrm{s} = 2500$ kJ/kg and the latent heat of fusion $r_\mathrm{i} = 333$ kJ/kg dominate in Eqs. (A.9a) and (A.9b).

Eq. (A.8) reads after these simplifications

$$\dot{m}_\mathrm{a} c_{pa}\frac{\mathrm{d}T_\mathrm{a}}{\mathrm{d}x}\,\mathrm{d}x = \dot{m}_\mathrm{ae} c_{pa}(T_\mathrm{ae} - T_\mathrm{a}) - \dot{m}_\mathrm{iv}(r_\mathrm{s} + r_\mathrm{i}) + \dot{Q} \tag{A.11}$$

The last equation reads after some algebraic rearrangements involving the equation of continuity

$$\frac{H}{T_\mathrm{a}}\frac{\mathrm{d}T_\mathrm{a}}{\mathrm{d}x} = \beta\left(1 - \frac{T_\mathrm{a}}{T_\mathrm{ae}}\right) - \frac{\dot{m}_\mathrm{iv}}{\dot{m}_\mathrm{a}}\frac{H}{\mathrm{d}x}\frac{r_\mathrm{s} + r_\mathrm{i}}{c_p T_\mathrm{a}} + \frac{\gamma - 1}{\gamma}\frac{\dot{q}}{pu} \tag{A.12}$$

Air entrainment and the melting of ice influence the mass fraction of ice $x_\mathrm{i} = \dot{m}_\mathrm{i}/\dot{m}_\mathrm{a}$. When x_i is differentiated with respect to x and combined with Eqs. (3.1) and (3.2), we obtain

$$\frac{\mathrm{d}x_\mathrm{i}}{\mathrm{d}x} = -\frac{\dot{m}_\mathrm{iv}}{\dot{m}_\mathrm{a}}\frac{1}{\mathrm{d}x} - \beta x_\mathrm{i}\frac{T_\mathrm{a}}{T_\mathrm{ae}}\frac{1}{H} \tag{A.13}$$

After elimination of $\dot{m}_\mathrm{iv}/\dot{m}_\mathrm{a}$ from Eqs. (A.12) and (A.13), we obtain

$$\frac{\mathrm{d}x_\mathrm{i}}{\mathrm{d}x} = -\beta\left[\left(1 - \frac{T_\mathrm{a}}{T_\mathrm{ae}}\right)\frac{c_5}{H} + \frac{x_\mathrm{i}}{H}\frac{T_\mathrm{a}}{T_\mathrm{ae}}\right] + \frac{c_5}{T_\mathrm{a}}\frac{\mathrm{d}T_\mathrm{a}}{\mathrm{d}x} - \frac{\gamma - 1}{\gamma}\frac{\dot{q}}{pu}\frac{c_5}{H} \tag{A.14}$$

with $c_5 = c_p T_\mathrm{a}/(r_\mathrm{i} + r_\mathrm{s})$.

The mass fraction of ice at the inlet of the control volume can be estimated by means of

$$x_i = x_{is} + \frac{dx_i}{dx} l \tag{A.15}$$

The system of equations (A.14) and (A.15) can be solved with respect to dx_i/dx and x_i.

References

[1] J.S. Puttock, G.W. Colenbrander, D.R. Blackmore, Maplin Sands Experiments 1980: Dispersion Results from Continuous Releases of Refrigerated Liquid Propane, Heavy Gas and Risk Assessment II, Reidel, 1983.

[2] D.L. Ermak, H.C. Goldwire, W.J. Hogan, R.P. Koopman, T.G. McRae, Results of 40 m^3 LNG Spills onto Water, Heavy Gas and Risk Assessment II, Reidel, 1983.

[3] M. Nielsen, S. Ott, Heat transfer in large-scale heavy-gas dispersion, J. Hazard. Mater. A67 (1999) 41–58.

[4] J.C. Statharas, A.G. Venetsanos, J.G. Bartzis, J. Würtz, U. Schmidtchen, Analysis of data from spilling experiments performed with liquid hydrogen, J. Hazard. Mater. A77 (2000) 57–75.

[5] R.E. Britter, J. McQuaid, Workbook on the Dispersion of Dense Gases, HSE Contract Research Report No. 17, 1988.

[6] J.P. Kunsch, T.K. Fanneløp, Unsteady heat-transfer effects on the spreading and dilution of dense cold clouds, J. Hazard. Mater. 43 (1995) 169–193.

[7] A. Kumar, A. Mahurkar, A. Joshi, Study of the spread of a cold instantaneous heavy gas release with surface heat transfer and variable entrainment, J. Hazard. Mater. B101 (2003) 157–177.

[8] G. Andreiev, D.E. Neff, R.N. Meroney, Heat Transfer Effects During Cold Dense Gas Dispersion, Gas Research Institute, Chicago, Illinois, Report No. GRI-83/0082, 1983.

[9] D.E. Neff, R.N. Meroney, J.L. Cermak, Wind Tunnel Study of Negatively Buoyant Plume due to an LNG Spill, CER 76-77 DEN-RNM-JSC 22, Colorado State University, 1976.

[10] P.T. Tokumaru, P.E. Dimotakis, Image correlation velocimetry, Exp. Fluids 19 (1995) 1–15.

[11] G.E.A. Meier, Computerized background-oriented schlieren, Exp. Fluids 33 (2002) 181–187.

[12] S.B. Dalziel, G.O. Hughes, B.R. Sutherland, Whole-field density measurements by 'synthetic schlieren', Exp. Fluids 28 (2000) 322–335.

[13] M. Ruff, F. Zumsteg, T.K. Fanneløp, Water content and energy balance for gas cloud emanating from a cryogenic spill, J. Hazard. Mater. 19 (1988) 51–68.

[14] R.K. Poag, Heat-transfer induced turbulent mixing in stably stratified shear flow, Ph.D. Thesis, University of Arkansas, 1987.

[15] O.S. Jensen, J.P. Kunsch, T. Rösgen, Optical density and velocity measurements in cryogenic gas flows, Exp. Fluids 39 (2005) 48–55.

[16] M.J. Moran, H.N. Shapiro, Fundamentals of Engineering Thermodynamics, third ed., John Wiley and Sons, Inc., 1995.

[17] G.H. Jirka, Turbulent buoyant jets and plumes, in: W. Rodi (Ed.), HMT, vol. 6, Pergamon Press, 1982.

[18] H. Schlichting, Grenzschichttheorie, Verlag-Braun, Karlsruhe, 1965.

[19] R.E. Britter, Assessment of the Use of Cold Gas in a Windtunnel to Investigate the Influence of Thermal Effects on the Dispersion of LNG Vapour Clouds, CUED/A-Aero/TR 14, Engineering Department, Cambridge University, 1987.

[20] H. Abrahamsson, On turbulent wall jets, Ph.D. Thesis, Chalmers University Göteborg, Sweden, 1997.

[21] J.P. Holman, Heat Transfer, fourth ed., McGraw-Hill, 1976.

[22] F. Zumsteg, Laborversuche zur instationären Ausbreitung kalter Gaswolken, Diss. ETHZ Nr. 8644, Institute of Fluiddynamics, ETHZ, 1988.

[23] T.K. Fanneløp, O. Jacobsen, Gravitational spreading of heavy-gas clouds instantaneously released, J. Appl. Math. Phys. (ZAMP) 35 (July) (1984).

[24] T.O. Spicer, J.A. Havens, in: S. Hartwig (Ed.), Development of a Heavier-Than-Air Dispersion Model for the U.S. Coast Guard Hazard Assessment Computer System, Heavy Gas and Risk Assessment III, Reidel, 1986.